Light Metals 2014
Edited by: John Grandfield
TMS (The Minerals, Metals & Materials Society), 2014

ON THE INFLUENCE OF MHD DRIVEN CONVECTION ON CATHODE WEAR

Kristian Etienne Einarsrud[1], Egil Skybakmoen[1], Asbjørn Solheim[1]
[1]SINTEF Materials and Chemistry, N-7465 Trondheim, Norway

Keywords: Cathode wear, MHD, current density, mass transfer.

Abstract

Non-uniform cathode wear observed in industrial aluminium reduction cells limits the cell life and thus presents a great challenge for the industry. The mechanism for cathode wear is not fully understood, although current densities, bath and metal convection and dissolution of aluminium carbide appear to play an important role. This work describes the two phase magnetohydrodynamic (MHD) flow in a simplified representation of an electrolysis cell, with emphasis upon the flow conditions at the cathode surface, which in turn drive mass transfer which is used to determine the cathode wear. Different cases are considered, focusing on current density distribution and electrode topology, simulating different operational conditions. The overall shape and magnitude of the wear rate obtained in the current simulations correspond well with measured wear rates, indicating that the MHD flow close to the cathode can shed new light upon cathode wear.

Introduction

Non-uniform wear observed in industrial aluminium cells with graphitized cathodes limits the cell life and thus presents a great challenge for the industry. Typically, the wear profile in a cross section of the cathode has been described as a double-w [1, 2, 3]. According to [3], the mechanism for the observed wear pattern is not fully understood. It seems clear however, that current densities (higher wear is typically observed in regions with high current density) and metal movement plays an important role, together with the formation, dissolution and transport of aluminium carbide, cf. [4].

Whatever the mechanism, knowledge of the local mass transfer coefficient is imperative in order to determine local wear rate, e.g. an analysis of the flow behaviour close to the carbon cathode is needed. The hydrodynamics of an industrial cell are governed by gravity, owing to density differences, and Lorentz forces, arising due to the mutual interaction of electromagnetic fields. As seen in several previous studies, e.g. [5, 6, 7], the flow in the metal is mainly governed by the Lorentz forces, i.e. it is a magnetohydrodynamic (MHD) flow.

From a qualitative point of view, measured wear patterns correspond well to typical MHD-induced flow patterns in the molten metal, as shown in Figure 1.

As seen from Figure 1, the flow is intensified in specific regions of the cell and the highest velocities and gradients thereof are typically obtained close to the edges of the cell, coinciding well with the regions with high observed wear rates. The flow pattern depicted in Figure 1 is based on the MHD benchmark case described by Severo et al. [6], in which a parabolic distribution of current density is applied on the cathode surface, with maximum towards the long sides of the cathode. Evidently, regions with intensified flow and high observed wear rates are correlated with regions of high current density as well.

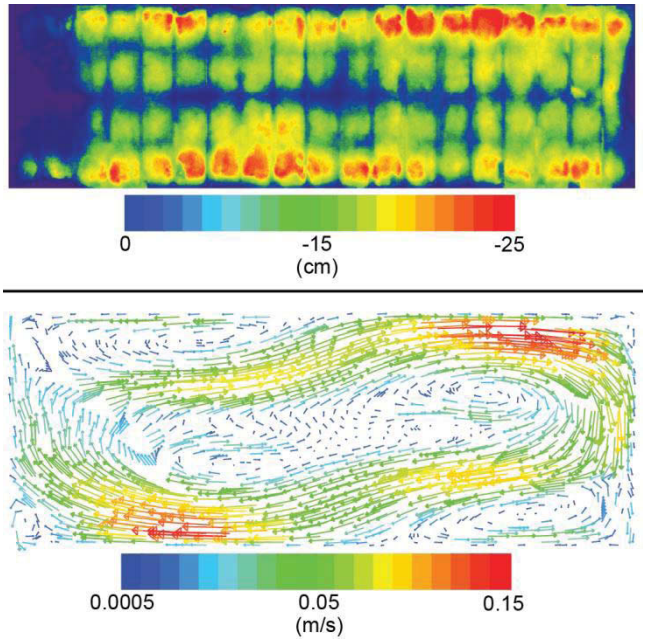

Figure 1. Measured wear [3] (top) and typical flow field in metal as of MHD benchmark proposed by [6] (bottom).

The striking similarity between the two figures above may of course be coincidental, and detailed simulations of the flow pattern in the specific cell are needed in order to explain the details of measured wear. Although the flow pattern in a specific industrial cell in principle could be calculated with (detailed) knowledge of the external magnetic fields and cell conditions, the objective of the current work is more general.

To the authors best knowledge, MHD induced convection in the bath has previously not been linked to cathode wear, at least not in the open literature. This paper will describe models and preliminary simulations on simplified representations of electrolysis cells, in order to shed light upon the importance of these phenomena.

Owing to the general scope, detailed issues related for instance to contact resistances in the busbars and how this influences current densities will not be considered. The focus will instead be on transparent and easily implementable conditions, from which future knowledge can be built.

MHD and Fluid Flow

Electric and magnetic fields (here respectively denoted $\boldsymbol{E}$ and $\boldsymbol{B}$) are governed by the Maxwell equations (cf. [8]) and constitutive closure relations. The closure relation used in the present work is

the continuum form of Ohm's law, stating that the electrical current density $\boldsymbol{j}$ is given as

$$\boldsymbol{j} = -\sigma\nabla\phi + \sigma\boldsymbol{u} \times \boldsymbol{B} \quad (1)$$

where $\boldsymbol{u}$ is the velocity of a fluid with electrical conductivity σ and ϕ is the electrical potential. The current density is of fundamental importance as it drives the principal electrochemical reactions in the cell and generates magnetic fields by induction. The mutual interaction between the current density and magnetic fields results in an electromagnetic force density, the Lorentz force, which for a fluid with no net electrical charge can be written as

$$\boldsymbol{f_L} = \boldsymbol{j} \times \boldsymbol{B} \quad (2)$$

The magnetic field can conveniently be calculated by solving the following Poisson equation for the magnetic vector potential

$$\nabla^2 \boldsymbol{A} = -\mu_0 \boldsymbol{j} \quad (3)$$

and

$$\boldsymbol{B} = \nabla \times \mathbf{A} + \boldsymbol{B}_{\text{ext}} \quad (4)$$

where $\boldsymbol{B}_{\text{ext}}$ is an external magnetic field, i.e. generated due to electrical currents outside of the considered domain. Equation 3 combined with conservation of electrical charge, $\nabla \cdot \boldsymbol{j} = 0$, and the constitutive closure relations given by Equations 1 and 2 yield a closed system of equations for the electromagnetic part of the current MHD model.

The second part of the proposed MHD model concerns fluid flow, here treated by an n-phase Volume of Fluid (VOF) model. The conservation of mass for the k-th phase (with density ρ_k) is written as

$$\partial_t \rho_k \alpha_k + \partial_i \rho_k \alpha_k u_i = 0 \quad (5)$$

where α_k is the volume fraction of the phase in question. Conservation of momentum is governed by the Navier-Stokes equations:

$$\partial_t \rho_k u_i + \partial_j \rho_k u_j u_i = -\partial_i p + \partial_j \mu_e \partial_j u_i + \rho_k g_i + (j \times B)_i \quad (6)$$

where $\mu_e = \mu_k + \mu_T$ is the effective viscosity arising from molecular and turbulent viscosities, g_i is gravity and $(j \times B)_i$ is the i-th component of the Lorentz force density.

Material properties (generically denoted ψ), such as for instance the electrical conductivity, are determined by local phase distributions and an appropriate weighting scheme, i.e.

$$\psi = \psi(\boldsymbol{x}, t) = \psi(\alpha_k) \quad (7)$$

The above set of equations yields a full coupling between all fields in question and constitutes a full MHD framework. Further details on the proposed framework as well as relevant verification studies can be found in [9].

Model Assumptions and Parameters

For simplicity, the presence of gas bubbles is neglected at the current stage, resulting in a two phase system consisting of molten bath and aluminium.

The mass transfer coefficient k proposed by Davies [10, 11], and later adopted by Haarberg, Solheim and Johansen [12], for turbulent flow parallel to a smooth wall is taken as a basis for the current calculations:

$$k = 0.075 \cdot Sc^{-2/3} u_\tau \quad (8)$$

where

$$Sc = \frac{\nu_{Al}}{D_i} \quad (9)$$

is the Schmidt number based on the kinematic viscosity of aluminium and the diffusivity of the (carbon containing) species, typically assumed to be carbide, in aluminium, and

$$u_\tau = \sqrt{\nu_{Al}|S|} \quad (10)$$

is the friction velocity of aluminium (on the cathode surface), calculated from the local strain rate S.

Given the mass transfer coefficient, the mass flux of carbon containing species at the cathode is given as

$$\dot{M} = k\Delta C \approx k C_{sat} \quad (11)$$

where it as a first approximation is assumed that the concentration difference between the cathode surface and bulk can be written as the saturation concentration C_{sat}, e.g. the surface is fully saturated while the bulk is fully depleted. The wear rate of the cathode (in m/s) is given directly from the local mass flux as:

$$\dot{W} = \frac{\dot{M}}{\rho_{cath}} \quad (12)$$

where ρ_{cath} is the density of the cathode material. All material properties required for the above equations are taken from [4] and [9] and summarized in Table I.

Table I. Summary of material properties.

Property	Symbol	Value	Unit
Bath conductivity	σ_{bath}	200	$(\Omega\text{cm})^{-1}$
Metal conductivity	σ_{Al}	$3{\cdot}10^6$	$(\Omega\text{cm})^{-1}$
Anode conductivity	σ_{Anode}	$3{\cdot}10^5$	$(\Omega\text{cm})^{-1}$
Bath density	ρ_{bath}	2070	kg/m^3
Metal density	ρ_{Al}	2170	kg/m^3
Bath viscosity	μ_{bath}	0.0033	kg/m·s
Metal viscosity	μ_{Al}	0.000868	kg/m·s
Diffusivity	D_i	$1{\cdot}10^{-8}$	m^2/s
Saturation concentration	C_{sat}	0.066	kg/m^3
Cathode density	ρ_{cath}	1650	kg/m^3

Setup of Simulations

The following simulations are, for the sake of simplifying the boundary conditions of the magnetic vector potential, performed on cylindrical system consisting of bath, metal and a solid anode, as sketched in Figure 2.

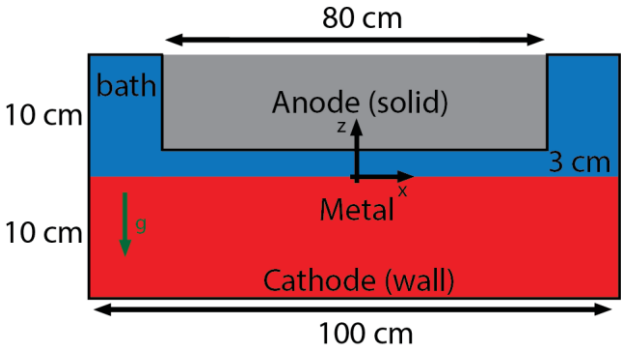

Figure 2. Sketch of computational domain with dimensions and initial distribution of phases.

The above domain is meshed with 420000 quadrilateral cells with enhanced resolution (1 mm) on the bath-metal and metal-cathode interfaces.

All of the following simulations are performed in ANSYS FLUENT R14 [13], using the 3D, double precision, pressure based transient solver. The momentum equations are discretized using the second order upwind scheme, while the PRESTO!-scheme is used for pressure. Pressure velocity coupling is performed by means of the default PISO-scheme. Turbulence is modelled by the realizable k-ϵ model with standard wall functions and the corresponding equations are discretized using the second order upwind scheme. Gradients are calculated based on a Green-Gauss cell based scheme, with distance weighting of diffusivities enabled. The transient formulation is first order implicit, with a constant time step of 0.05 s.

The multiphase nature of the flow is treated by the explicit VOF method with implicit body forces, discretized using the PLIC-scheme. Equations are solved with bath as reference density.

Electromagnetic fields are treated as UDS-equations, as described in [9], discretized using a Power-law scheme. In order to enhance convergence for the electrical potential, the W-cycle is employed for this equation. Remaining equations are solved using the Flexible cycle.

All boundaries enclosing the system are treated as no-slip walls. For the electrical potential, the bath-anode interface is treated as a coupled boundary while the cathode is given a specified electrical current density. A constant reference potential is given on the top surface of the anode. All other surfaces are assumed to be non-conducting.

Dirichlet boundary conditions corresponding to a cylindrical current density are specified for the z-component of the magnetic vector potential (the principal component)

$$A_{z,bc} = -\frac{\mu_0 j_0 (x^2+y^2)}{4} \tag{13}$$

while academic boundary conditions are used for the remaining components,

$$A_{i\neq z,bc} = 0 \tag{14}$$

Details, verification and further justifications of the above boundary conditions can be found in [9].

Gravity is enabled for all simulations, pointing in the negative z-direction.

Simulations are run for 200 s flowtime in order to ensure that a statistically steady state is reached.

Results

In order to investigate the influence of MHD-flow, several different cases are defined, each showing a simplified representation of features found in an industrial cell. The main focus will be on the influence of current distribution on the cathode, as high current density regions are expected to be correlated to regions with high wear rates.

Uniform Cathode Current Density

The first case is defined with a uniform current density $j_0 = 8000$ A/m^2 on the cathode surface. As the principal current density is in the negative z-direction, the resulting induced magnetic field will be mainly tangential to the system, thus resulting in a radial Lorentz force and consequently a radial pressure distribution, when considering only the induced magnetic field. External magnetic fields are not considered in this case.

As the anode is smaller than the cathode in the geometry specified, the current distribution will be different in the two phases considered (due to the large difference in conductivity). Consequently, the distribution of Lorentz forces will also be different, allowing for fluid flow.

A uniform current density is not expected to be a good representation of reality, where the current is known to be distributed on the cathode surface, both due to physical effects and by design. Nevertheless, this case serves as an important proof of concept and reference for simulations with more realistic conditions.

The predicted magnetic field on the cathode and velocity distribution in the zx-plane is shown in Figure 3. As seen from the figure, the magnetic field is clockwise and increasing towards the perimeter of the cell, as expected. The unequal distribution of Lorentz force density between the bath and the metal results in a counter-clockwise toroidal flow pattern in the metal, with high intensity close to the (projected) anode edge. It should be noted that a flow pattern parallel to the induced magnetic field is not observed in the current case, owing to the weak coupling between vertical magnetic fields (it is mainly tangential in this case) and radial currents.

From the predicted flow pattern, the wear rate (in cm/year) can be predicted from Equation 12. The predicted wear rate is shown in Figure 4, showing a "single-W" profile with maximum close to the projected anode edge. The predicted wear rate (2 cm/year) corresponds well to measured maximum values of 1-3 cm/year, cf. [3].

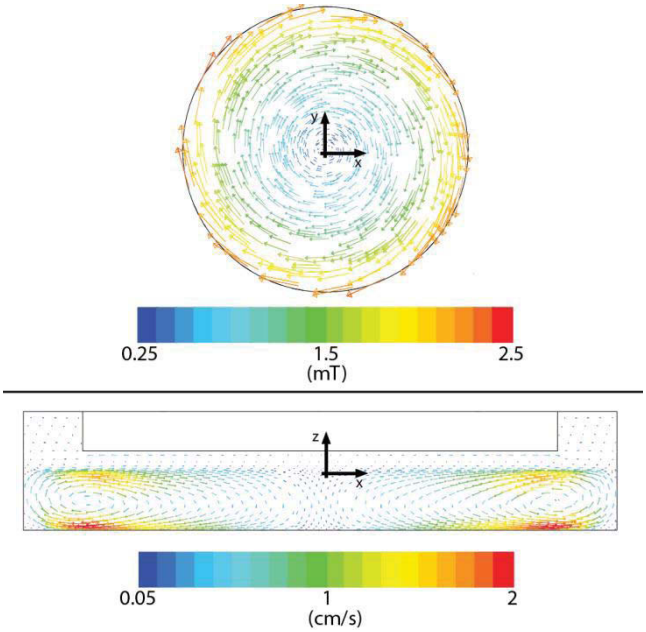

Figure 3. Predicted magnetic field (top) and flow field (bottom) for case with uniform current density on cathode.

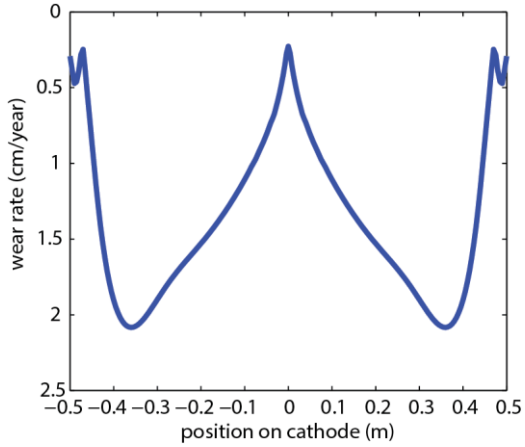

Figure 4. Predicted wear rate on cathode surface for case with uniform cathode current density.

Distributed Cathode Current Density

Due to heat losses, a side-ledge of frozen bath will form on the inside of a cell. For a poorly designed cell, the side ledge can stretch far beneath the anode shadow. This region is characterized by poor electrical conductivity and thus forces the electrical current towards central regions of the cathode. As the region of the cathode covered by the side ledge is rendered inactive (both electrochemically and flow-wise), low wear rates are expected as indicated also from the measurements shown in...

The inactive region on the edges of the cathode can be extended further due to the presence of sludge (consisting of alumina particles with frozen bath), which, due to convection will be transported toward the edges of the cell.

In addition to the features forcing the current towards central regions of the cell, competing features tend to force the electrical current towards the outer regions of the cell. The two most significant contributions are the collector bars (responsible for collecting electrical current and transporting it to the next cell) and sludge, which due to typical feeder positioning, is generated in central parts of the cell.

A current density distribution capturing the above effects is proposed as

$$j(r) = a \cdot \sin(2\pi|r|) \cdot (r_{max} - |r|) \tag{15}$$

where $r = \sqrt{x^2 + y^2}$ is the (radial) position on the cathode surface with maximal radius $r_{max} = 0.5$ m and a is a normalization factor determined by

$$2\pi \int_0^{r_{max}} j(r)dr = j_0 A_{cath} \tag{16}$$

i.e., the total electrical current is identical to the uniform case. The imposed current density is shown in Figure 5 for reference, while the predicted flow field and wear rate is shown in Figure 6.

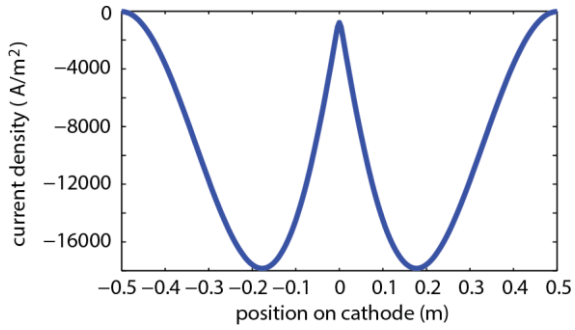

Figure 5. Imposed cathode current density.

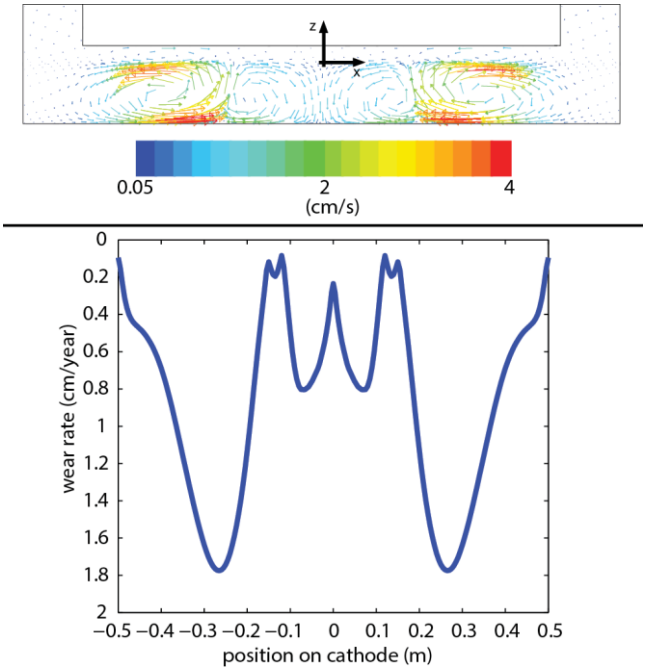

Figure 6. Predicted flow field (top) and wear rate for the case with distributed cathode current density.

As seen from Figure 6, the proposed current density distribution results in two toroidal flow structures, the innermost flowing counter clockwise, corresponding to the uniform case, and one

flowing clockwise with higher intensity. The resulting predicted wear rate is a "double-w", with global maximum close to the maximum current density and outer vortex in the flow field. In addition, a distinct local maximum in the wear rate is observed close to the inner flow vortex, which clearly is not linked directly to high local current densities.

Non-Uniform Anode

In the measured wear shown in Figure 1, the interanode and centre-channel gaps are clearly visible as regions with comparably less wear than regions directly beneath the anode. Although the above results indicate an influence of the simulated side-channel, it is worthwhile to investigate the influence of a centre-channel as well. In the current setting, this is simulated by introducing a hole in the anode, with diameter 15 cm. All other conditions are kept as for the uniform cathode current case. The resulting flow and wear pattern is shown in Figure 7.

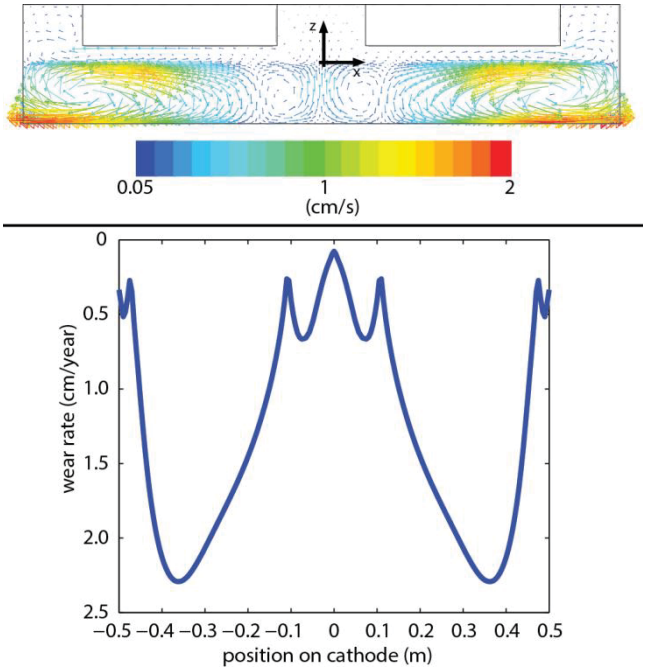

Figure 7. Predicted flow field (top) and wear rate for case with simulated centre channel.

As for the case with a distributed current density, the case with a simulated centre channel results in a "double-w" wear pattern. The global maximum is however higher than the distributed current case. Moreover, the direction of the two vortices is inverted, meaning that a combination of the above anode geometry and the previously proposed current density distribution could promote overall lower wear rates. The wear rate pattern shown in Figure 8 is obtained with both conditions met and confirms that this is the case.

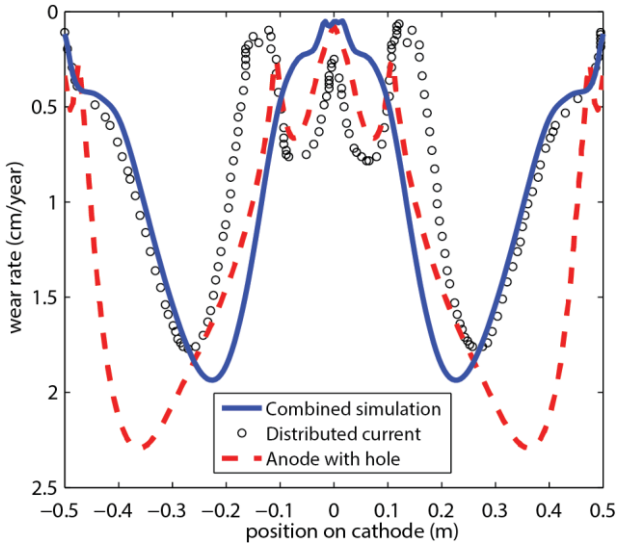

Figure 8. Wear pattern predicted for simulation with both non-uniform anode and distributed current density (solid line), compared to cases with separated phenomena (dashed lines and symbols).

Non-Uniform Cathode

Finally, the influence of a preworn cathode is considered. Owing to the long expected simulation times required to obtain a worn cathode surface and numerical challenges related to dynamic boundaries, simulations are at the current stage performed on a predefined (simplified) cathode profile, consisting of a 2 cm deep ring on the cathode surface. All horizontal surfaces on the cathode are assumed to carry a uniform current density corresponding to the uniform case. The predicted flow and wear pattern is shown in Figure 9.

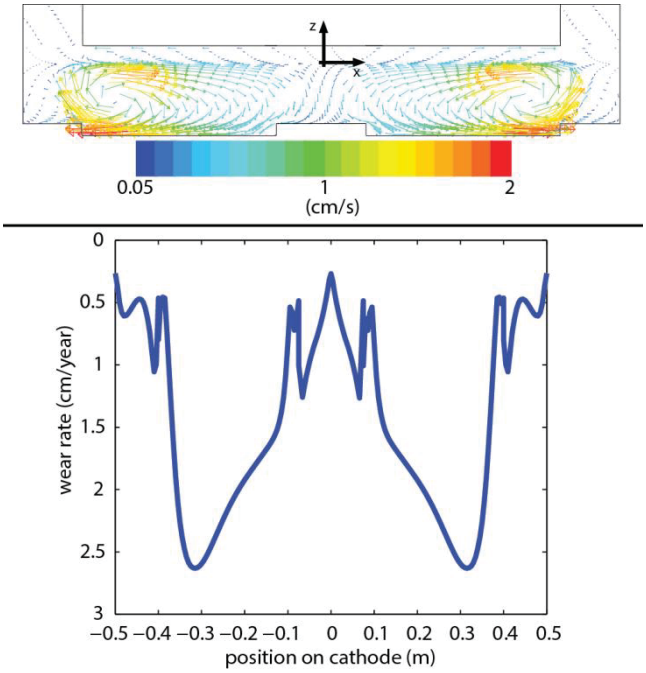

Figure 9. Predicted flow field (top) and wear rate (bottom) with preworn cathode.

Corresponding to previously studied cases with uniform cathode current density, simulations on a system with a predefined cathode structure show the formation of a toroidal counter-clockwise flow structure. Due to the abrupt changes in cathode topology, the flow becomes equivalent to that of a facing step, where increased strain and consequently mass transfer coefficients are expected, resulting, again, in a "double-w" type of wear profile.

Summary and Conclusions

The current work sets out to link the industrially observed cathode wear pattern to local magnetohydrodynamic flow, through a description of local mass transfer coefficients. Simulations have been performed on four cases, representing idealized conditions thought to occur in a typical industrial cell. Results indicate that different wear patterns can be obtained by altering the current density, either directly or indirectly by altering the electrode topology.

A uniform cathode current density promotes, under the given assumptions, a single w wear pattern, while idealized representations of more realistic conditions such as a distributed current density and altered electrode topologies tend to result in a double-w profile, corresponding well to measured profiles.

Basing required material constants upon those obtained for aluminium carbide, the predicted magnitude of the wear rate (1-3 cm per year) corresponds well to those estimated from measurements, in addition to the expected shape.

Although idealized in many senses, in particular with respect to geometry and treatment of the current density distribution within the cathode, the current work highlights that MHD-driven convection potentially can explain the observed non-uniform wear pattern. Extended simulations with a relaxed degree of idealization are required to confirm this, justified by the current work. If such large scale, detailed simulations prove successful, the process of bus- and collector-bar design could be reconsidered to include compensation of cathode wear in addition to MHD stability issues, potentially increasing the cell lifetime, as indicated by Figure 8.

Acknowledgements

The present work was carried out in Durable Materials in Primary Aluminium Production (DuraMat) project, financed by the Research Council of Norway, Hydro Primary Metal Technology, Sør-Norge Aluminium (Søral) and Elkem Carbon. Permission to publish the results is gratefully acknowledged.

References

1. M. Sørlie and H.A. Øye, "Cathodes in Aluminium Electrolysis", 2010, Aluminium Verlag.
2. P. Reny and S. Wilkening, "Graphite Cathode Wear Study at Alouette", *Light Metals 2000*, pp. 399-405.
3. E. Skybakmoen, S. Rørvik, A. Solheim, K.R. Holm, P. Tiefenbach and Ø. Østrem, "Measurement of cathode surface wear profiles by laser scanning", *Light Metals 2011*, pp. 1061-1066.
4. A. Solheim, "Some hypothesis concerning cathode wear in aluminium electrolysis cells", *COM-Light Metals*, 2011.
5. M.M. Bilek, W.D. Zhang, and F.J. Stevens, "Modelling of Electrolyte Flow and Its Related Transport Processes in Aluminium Reduction Cells", *Light Metals 1994*, pp. 323-331.
6. D.S. Severo, V. Gusberti, A.F. Schneider, E.C.V. Pinto and V. Potocnik, "Comparison of various methods for modeling the metal-bath interface", *Light Metals 2008*, pp. 413-418.
7. V. Bojarevics and K. Pericleous, "Solutions for the metal-bath interface in aluminium electrolysis cells", *Light Metals 2009*, pp. 569-574.
8. D.J. Griffiths, "Introduction to Electrodynamics, Third edition", *1999*, Prentice Hall.
9. K.E. Einarsrud, "A Treatise on Interpolar Transport Phenomena", *PhD Thesis 2012:201,* Norwegian University of Science and Technology (NTNU).
10. C.N. Davies, "Turbulence Phenomena", 1972, Academic Press.
11. C.N. Davies, "A new theory of aerosol deposition from turbulent flow", *Chemical Engineering Science*, 38 (1983) pp. 135-139.
12. T. Haarberg, A. Solheim and S.T. Johansen, "Effect of Anodic Gas Release on Current Efficiency in Hall-Héroult Cells", *Light Metals 1998*, pp. 475-481.
13. ANSYS. *ANSYS – Simulation Driven Product Development – www.ansys.com.* 2013 October.